Communication

Enhanced Hydrogen Evolution Reaction of a Zn^{+2}-Stabilized Tungstate Electrocatalyst

Dasu Ram Paudel [1],*[ID], Gopi Chandra Kaphle [2][ID], Bhoj Raj Poudel [1][ID], Mukunda KC [2], Manjinder Singh [3][ID] and Gunendra Prasad Ojha [4],*[ID]

1   Department of Chemistry, Tri-Chandra Multiple Campus, Tribhuvan University, Kathmandu 44613, Nepal; bhoj.poudel@trc.tu.edu.np
2   Materials Science and Computational Nano Lab, Central Department of Physics, Tribhuvan University, Kathmandu 44613, Nepal; gck223@gmail.com (G.C.K.); kshetriji@gmail.com (M.K.)
3   Department of Chemical and Molecular Engineering, Hanyang University ERICA, Ansan 15588, Republic of Korea; manroop76@gmail.com
4   Department of Chemistry and Physics, Prairie View A&M University, Prairie View, TX 77446, USA
*   Correspondence: dasu.paudel@trc.tu.edu.np (D.R.P.); gpojha10@gmail.com (G.P.O.)

Abstract: Due to their diverse properties and functionalities, cost-effective transition metal-based nanomaterials have been rigorously studied for electrochemical applications. Ultrathin nanosheets have been identified as the most effective electrodes for catalyzing water-splitting reactions in both acidic and alkaline environments. Here, we reported ZnWO$_4$, a member of the tungstate family, as an effective electrocatalyst for promoting the electrochemical hydrogen evolution reaction. The Zn^{+2}-stabilized tungstate showed a remarkable cathodic reaction during the water-splitting reaction with low overpotential (136 mV at 10 mA cm^{-2}) and small HER kinetics (Tafel Slope = 75.3 mV dec^{-1}) and long-term cyclic durability. The high-valence tungsten stabilized with divalent Zn^{+2} promotes electron transfer during the reaction, making it an advanced electrocatalyst for green hydrogen production.

Keywords: tungstate; green hydrogen; electrocatalysis; HER

1. Introduction

Currently, the world is experiencing energy challenges resulting from the depletion of non-renewable fossil fuels [1–5]. The combustion of fossil fuels emits environmentally harmful gases such as CO$_2$, NO$_2$, and SO$_2$, which drive the rise in atmospheric greenhouse gas levels and intensify worldwide environmental concerns [6,7]. At present, the burning of fossil fuels is responsible for more than 85% of global greenhouse emissions [8]. Moreover, the excessive use of fossil fuels leads to the degradation of natural ecosystems, global warming, and ultimately the energy crisis [9,10]. The use of renewable and green energy sources is the key solution to achieve carbon neutrality and create a sustainable society [11]. Hydrogen energy has the potential to effectively address all aspects of energy usage and global environmental issues due to its wide range of applications with zero emissions [12]. The green hydrogen, a clean and sustainable energy source, produced from water-splitting reactions is endowed with great potential to convert electrical energy into fuels for later use [13]. The water electrolysis occurring at the electrode surface requires active catalysts to ensure a more energy-efficient process [14]. The impressive electrocatalytic behavior of Pt-based HER electrodes and Ru and Ir-based OER electrodes in water-splitting processes represents a promising opportunity for green hydrogen production [4,15]. However, large-scale commercial production with these rare, expensive, and unstable noble metal-based

catalysts is challenging. Thus, considerable efforts in developing a promising catalyst for practical green hydrogen production are urgently needed [16].

Earth-abundant element-based nanomaterials, mostly consisting of transition metals (TM), are expected to replace these state-of-the-art metals for commercial energy applications as catalysts [17]. The wide-ranging nanostructure of TM compounds like chalcogenides, oxides/oxyhydroxides, nitride/oxynitrides, phosphides, carbides, etc., with varying compositions such as single-phase, hetero-phase, composite, alloys, etc., is a topic attracting growing interest in advanced electrocatalysis research [4,18–20]. Tungstates have gained significant attention due to their exceptional catalytic and electrochemical properties [21,22]. Metal tungstates with high-valence W atoms show high electrical conductivity and excellent electrochemical performance [23]. Among the tungstates, zinc tungstate, a well-known n-type semiconductor and a member of the structurally related divalent transition metal tungstate family, crystallizes in a distorted triclinic wolframite structure where Zn and W atoms are octahedrally bonded to six oxygen atoms [24,25]. The Zn^{+2} ion-stabilized form of this tungstate, $ZnWO_4$, with a versatile electronic and molecular entity, reactivity, and stability, is a promising candidate for electrochemical activities [26,27].

Based on previous studies, the morphological properties are important determinants of nanomaterials' applications, such as in water-splitting reactions, supercapacitors, fuel cells, batteries, and nitrogen reduction reactions [28–30]. Among the many strategies used to tune an ideal morphology, various approaches like changing the precursor ratio, changing the reaction temperature, pH adjustment, the use of surfactants, ion impregnation, etc., are common [31]. Optimizing the molar ratios of divalent ions within tungstate nanostructures presents an exciting opportunity for enhancing nucleation processes. This innovative strategy could lead to significant advancements in material development. Additionally, it is notable that the electrochemical behavior of tungstates is positively affected by changes in the electronic structure induced by the bivalent metal (Zn^{+2}) on multivalent W atoms [32]. Metal tungstate ($CoWO_4$) nanoparticles demonstrate excellent activity as a bifunctional electrocatalyst for the hydrogen evolution reaction (HER) and oxygen evolution reaction (OER), according to Luo et al. [33]. Malavekar et al. [34] highlighted the promising capabilities of the $NiWO_4$ nanostructure as an OER electrode, noting its excellent ability to achieve reduced overpotential and Tafel slope values in alkaline media. This advancement suggests opportunities for further research on tungstate nanomaterials and development in enhancing electrode performance in electrochemical applications.

Hence, we adopt a facile hydrothermal method to synthesize ultrathin nanosheets of Zn^{+2}-stabilized WO_4^{-2} ($ZnWO_4$) using varying molar concentrations of Zn^{+2} ions for the HER in alkaline electrolytes. The resultant ultrathin nanosheets of $ZnWO_4$ with a molar ratio of 1:1 exhibit pronounced HER activity, surpassing that of the other catalysts and comparable to commercial Pt/C. This high activity is mainly associated with the large surface area of these nanosheets, the higher number of electroactive sites, the tunable Fermi level and d-band structure, and the synergistic effects of bimetals. Low-cost transition bimetallic oxides with suitable nanoarchitectures offer a promising solution for enhancing the hydrogen evolution reaction. This approach supports the pursuit of economical and sustainable energy solutions, making it a valuable area for further exploration and development.

2. Materials and Methods

2.1. Materials

Zinc nitrate hexahydrate ($Zn(NO_3)_2 \cdot 6H_2O$), sodium tungstate dihydrate, ($Na_2WO_4 \cdot 2H_2O$), urea (CH_4N_2O), ammonium fluoride (NH_4F), and potassium hydroxide (KOH) were purchased from Sigma-Aldrich, St. Louis, MO, USA. Nickel foam (Ni-foam) was purchased

from Taiyuan Liyuan Lithium Technology Co., Ltd., Taiyuan, China. All the chemicals were of analytical grade and were used as received.

2.2. Treatment of Nickel Foam

Firstly, the Ni foam substrate was cut into 5 cm × 2 cm pieces, which were then pretreated with a 2 M HCl solution in an ultrasonic bath for 30 min to remove the NiO layer from the surface. Subsequently, the substrates were washed several times with acetone, absolute ethanol, and deionized (DI) water.

2.3. Synthesis of ZnWO$_4$ Nanosheets on Ni Foam

ZnWO$_4$ ultrathin nanosheets were synthesized on nickel foam using a facile hydrothermal method. Firstly, a solution containing 1 mmol of Zn(NO$_3$)$_2$·6H$_2$O, 1 mmol of Na$_2$WO$_4$·2H$_2$O, 3 mmol of urea (CH$_4$N$_2$O), and 0.5 mmol of NH$_4$F in DI water (60 mL) was prepared with constant magnetic stirring for 30 min. The resulting solution was transferred to a 100 mL Teflon-lined stainless-steel autoclave and a piece of pretreated Ni foam (2 cm × 5 cm) was immersed in the reaction solution. The autoclave was sealed and maintained at 120 °C for 12 h followed by natural cooling to room temperature. The resultant product was washed carefully with DI water and ethanol to remove residual impurities and dried in an oven for 10 h. Finally, the dried material was annealed at 250 °C for 3 h in air. Similar conditions were applied for other samples of ZnWO$_4$ with a varying composition of the Zn precursor, i.e., 0.5 mmol and 2 mmol of the solution with 1 mmol of Na$_2$WO$_4$·2H$_2$O. The Ni foam was cut to the desired size (1 × 1 cm^2) on a cutting mat, ensuring smooth edges and minimal damage to facilitate subsequent electrochemical characterizations.

2.4. Material Characterizations

The crystalline properties of catalysts were examined by means of X-ray diffraction (XRD) with the standard of Cu Kα radiation from the 2θ range 10–80° in a scan range of 2 degree per minutes (λ = 0.154 nm) (Rigaku Co., Tokyo, Japan). The surface morphology and the energy dispersive X-ray spectroscopy (EDS)-based elemental composition of the electrode was observed by means of field-emission scanning electron microscopy (FE-SEM) on a Zeiss Supra 40VP system (Burgoberbach, Germany) using a piece of Ni foam.

2.5. Electrochemical Measurements

The electrochemical properties of the as-synthesized electrode materials were analyzed in a CHI 660E workstation. An Ag/AgCl (saturated with KCl solution) reference electrode, a graphite rod counter electrode, and the catalyst-loaded 1 cm × 1 cm Ni foam sample as the working electrode were set up in a three-electrode configuration, and the electrochemical performances were recorded in a 1 M KOH electrolyte solution. The catalytic activities for water splitting were assessed through HER activity using the linear sweep voltammetry (LSV) technique at a scan rate of 2.0 mV s^{-1} and were corrected by means of iR compensation (E$_{Corrected}$ = E$_{RHE}$ − iR$_s$, where i = current and R$_s$ = equivalent series resistance). The Tafel slopes of each individual catalyst were calculated [(η = a + $b$log$j$), where 'j' is the current density, and 'b' is the Tafel slope] to explore the electrode kinetics for water splitting via the HER reaction. The electrochemical impedance spectrum (EIS) and the Nyquist plots were measured over the frequency range (100 kHz to 0.01 Hz) at an amplitude of 5 mV. The electrochemically active surface area (ECSA) of catalysts was evaluated using cyclic voltammetry (CV) at different scan rates in the non-Faradaic region to determine the double-layer capacitance (C$_{dl}$). The measured potentials were standardized to the reversible hydrogen electrode (RHE) [E$_{(RHE)}$ = E^0$_{(Ag/AgCl)}$ + E$_{(Ag/AgCl)}$ + 0.059 × pH; E$_{RHE}$ = calculated potential vs. RHE, E$_{Ag/AgCl}$ = measured potential vs. Ag/AgCl, E^0$_{Ag/AgCl}$ = 0.197 V at 25 °C] [35].

3. Results and Discussion

The Zn-tungstate nanocatalyst was synthesized by means of a hydrothermal process followed by heat treatment as shown in Scheme 1 (for more detail, see the Materials and Methods section). The varying molar ratio of Zn^{+2} ions incorporated into the tungstate moiety $(WO_4)^{-2}$ enables the formation of the highly crystalline $ZnWO_4$ ultrathin nanosheets. The single-step hydrothermal method is beneficial for synthesizing highly stable nanocrystals at an ambient temperature and auto-generated pressure.
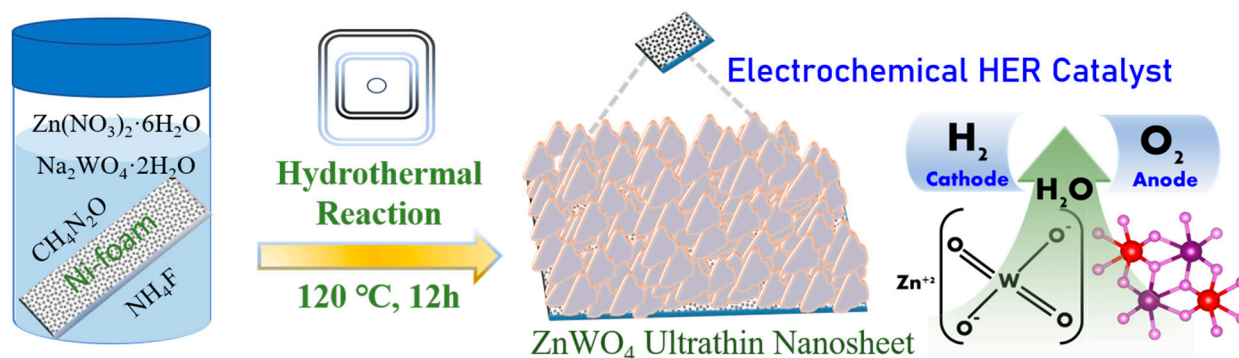
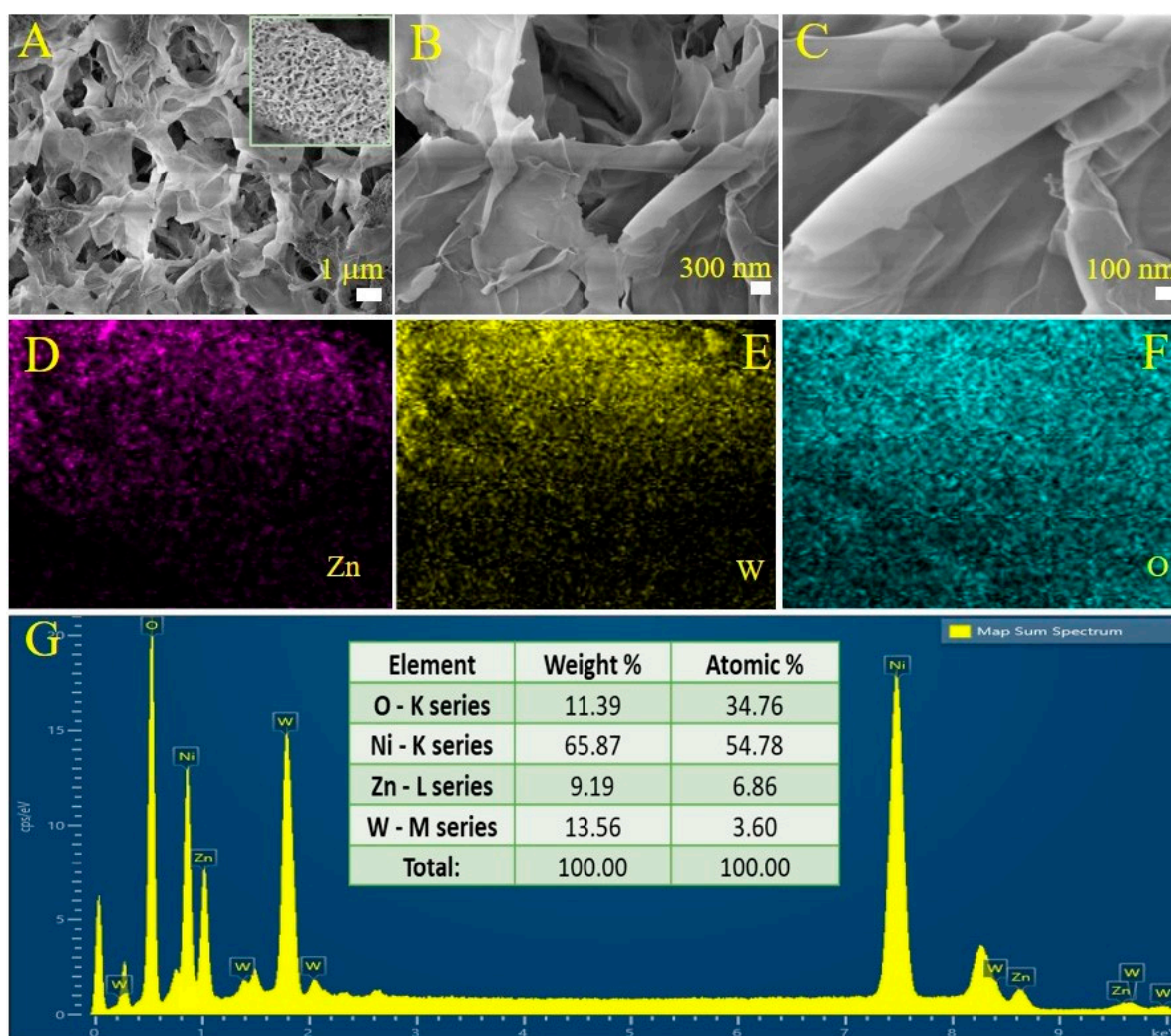**Scheme 1.** Schematic showing the synthesis of $ZnWO_4$ ultrathin nanosheets.

The crystallinity of the synthesized $ZnWO_4$ was assessed by means of X-ray diffraction (XRD) analysis (Figure 1). The strong diffraction peaks at 30.473 and 30.720 correspond to the (111) and (−111) crystalline planes, respectively, indicating the formation of the highly crystalline nanostructure of pure $ZnWO_4$ (JCPDF No. 15-0774). Other significant peaks at a 2θ angle of 18.9 (100), 23.9 (011), 24.6 (110), 36.3 (021), 36.5 (002), 53.9 (−202), 64.8 (−311) indicate the formation of the monoclinic sanmartinite crystal structure of $ZnWO_4$ with the space group P2/c(13) [25]. These structural properties of the tungstate indicate the long-distance structural organizations as well as the excellent crystallinity which imposes the best electrocatalytic properties due to the highly dispersed W and Zn atoms on the molecular scale [36].
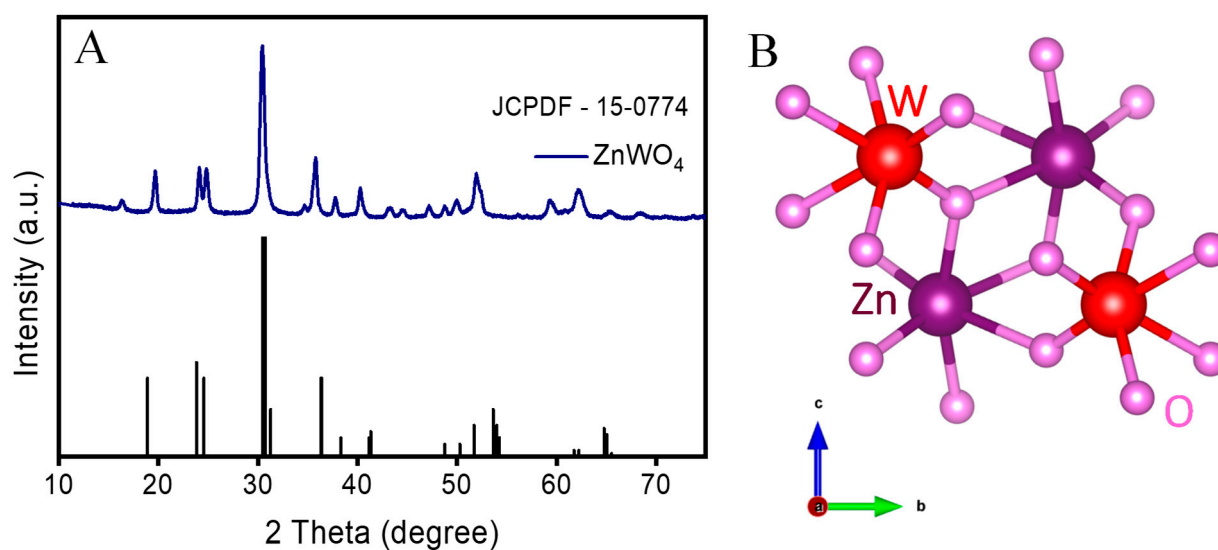
Figure 1. XRD crystallography of $ZnWO_4$ (**A**); monoclinic sanmartinite crystal structure of $ZnWO_4$ (**B**), generated from VESTA software (Version 3.5.2).

The microstructure of the synthesized sample with its characteristic morphology is depicted in Figure 2. The field-emission scanning electron microscopy (FE-SEM) images

with porous Ni foam as the supporting material of $ZnWO_4$ indicate the growth of homogeneously dispersed ultrathin nanosheets on the substrate (Figure 2A and inset) with an enormous porous architecture. The magnified FE-SEM images (Figure 2B,C) clearly show the layered spongy channels with thin sheets, which are ultimately beneficial for the electrochemical activity, offering a high specific surface area, faster charge transfer, and better conductivity. The ample porosity and the thin-edge layered structure allow the passage of the electrolyte during the electrochemical measurement, allowing for faster electrode kinetics and minimum charge resistance [37]. Moreover, the energy dispersive spectroscopy (EDS) elemental analysis of the sample showed the presence of all the constituent elements, i.e., Zn, W, and O, as shown by the element mapping images in Figure 2D,E,F, respectively. The EDS spectrum and its quantification results are shown in Figure 2G and the inset, indicating the presence of all the constituent elements in definite weight percentages and atomic percentages. Hence, the distinctively thinner morphology of $ZnWO_4$ nanosheets explicitly increases the number of accessible catalytic sites for interactions between the electrode and electrolyte. This leads to significantly improved electron transfer and reaction kinetics, resulting in superior electrochemical performance in hydrogen evolution reactions (HERs). The greater availability of these catalytic sites is a crucial factor driving the enhanced HER activity observed in these nanosheets, demonstrating their effectiveness and potential in the water-splitting process [4].

Element	Weight %	Atomic %
O - K series	11.39	34.76
Ni - K series	65.87	54.78
Zn - L series	9.19	6.86
W - M series	13.56	3.60
Total:	100.00	100.00

Figure 2. FESEM images of $ZnWO_4$ from low to higher magnification (**A**–**C**), FESEM-EDS color mapping images of $ZnWO_4$ (**D**–**F**), and EDS spectrum (**G**).

The electrocatalytic properties for water-splitting applications to produce green hydrogen are of great interest in recent energy conversion technology. To evaluate the electroactivity of the synthesized materials, we accessed different electrochemical parameters in an alkaline medium (1 M KOH). The 1 cm × 1 cm $ZnWO_4$-loaded nickel foam sample was used for all electrochemical measurements. The activation or surface cleaning of the electrocatalyst was carried out by running cyclic voltammetry (15 cycles) in a specific voltage range (in HER regions) at a relatively high scan rate before measuring the LSV or other electrochemical parameters [38].

The active sites of the electrode for ion adsorption were first quantified by performing the CV cycles in non-Faradaic potential regions. The slope for the linear plot of non-Faradaic currents (I_a - I_c) as a function of scan rate is the double layer capacitance ($C_{dl} = d(\Delta j)/dv$), which specifies the relative electrocatalytic activity of the respective catalyst, indicating the highly exposed active sites in terms of the active surface area, reported as the electrochemical active surface area (ECSA) [38]. The ECSA is linearly proportional to the C_{dl} and is calculated by employing the formula ECSA = C_{dl}/Cs, where Cs is the capacitance of a flat electrode. Figure 3A–C show the corresponding cyclic voltammograms of Zn^{+2} tungstate at a scan rate of 20–100 mV s^{-1}. The calculated C_{dl} value [$ZnWO_4$ (1:1) = 10.4 mF cm^{-2}, $ZnWO_4$ (0.5:1) = 8.8 mF cm^{-2}, $ZnWO_4$ (2:1) = 6.6 mF cm^{-2}] in Figure 3D indicates that the equimolar ratio of Zn:W (1:1) exhibited more active sites on the electrode and thus a larger ECSA. From these results, the specific activity of the electrocatalyst is enhanced due to the highly porous ultrathin network of $ZnWO_4$ nanosheets on nickel foam.
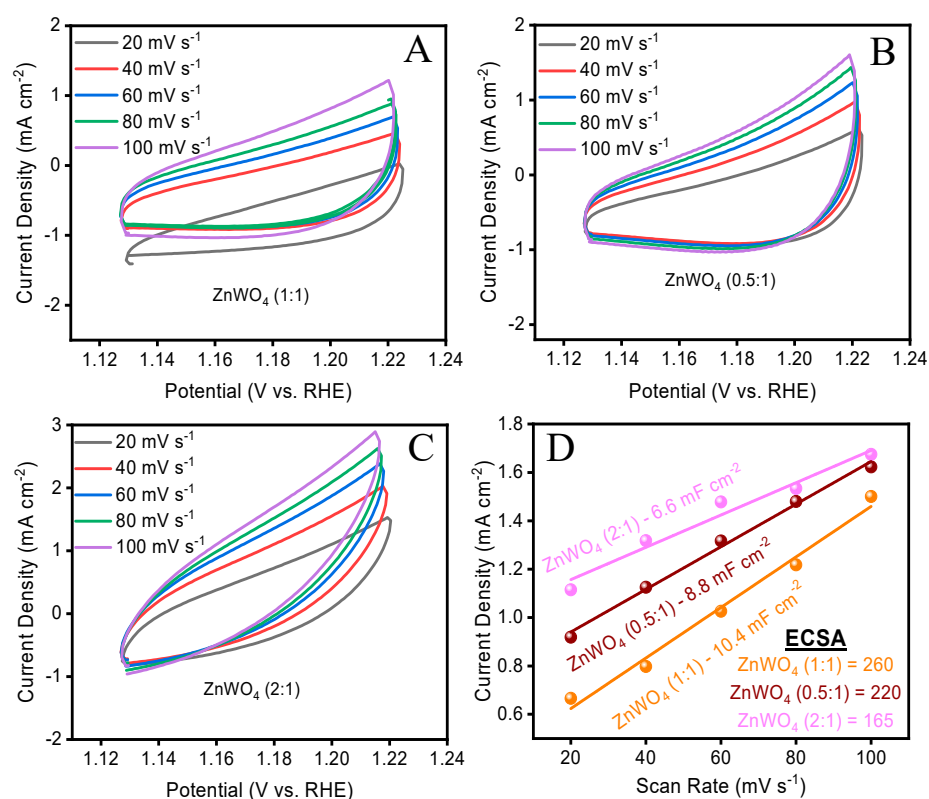
Figure 3. CV curves of as-synthesized electrodes at different scan rates (**A–C**), C_{dl} value, and the corresponding ECSA of the electrode (**D**).

The electrochemical water electrolysis performance of the developed catalyst was evaluated by the polarization curves obtained from the linear sweep voltammetry at a scan rate of 2 mV s^{-1} in a three-electrode system. Figure 4A shows the polarization curves

of the as-synthesized catalyst, commercial Pt/C, and the bare Ni foam with reference to the RHE after iR compensation. For all the catalysts, partial iR compensation (95%) was carried out to correct the voltage loss caused by the medium solution between the reference electrode and the working electrode, as well as to avoid potentiostat oscillation. The overpotential measured at the benchmark current density of 10 mA cm^{-2} for Pt/C is 35 mV, that for ZnWO$_4$ (1:1) is 136 mV, that for ZnWO$_4$ (0.5:1) is 192 mV, that for ZnWO$_4$ (2:1) is 252 mV, and for bare Ni foam, it is 298 mV (Figure 4B). The Zn^{+2} ion-stabilized tungstate showed a fairly good overpotential, showing a competitive electrochemical activity for HER application. The 1:1 ZnWO$_4$ catalyst showed better electrochemical performance than the other electrodes, conceivably due to its fine-tuned morphology, enormous porosity, strong electrode–electrolyte interactions, and more importantly its high-valence tungstate stabilized with divalent Zn^{+2} ions of high crystallinity [39].
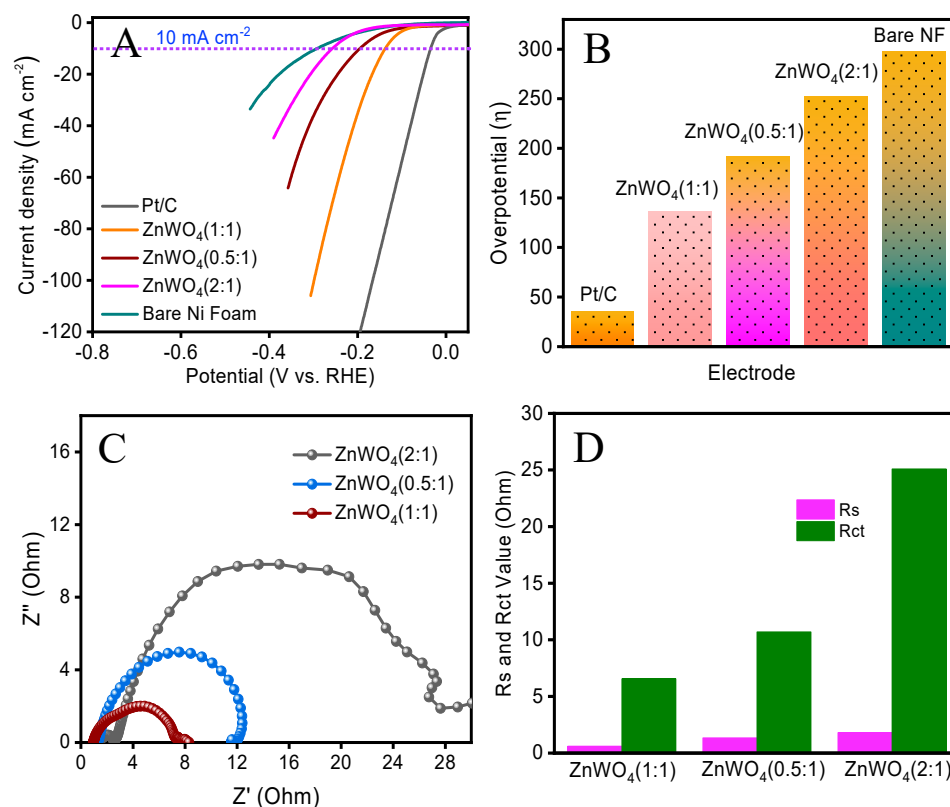

Figure 4. LSV polarization curves for the HER (**A**); corresponding overpotential (**B**); Nyquist plot of the developed catalyst and its respective R$_s$ and R$_{CT}$ values (**C,D**).

Figure 4C,D show the electrochemical impedance spectroscopy (EIS) measurements and the impedance responses of the as-synthesized catalyst, represented in Nyquist plots. The relative solution resistance (R$_s$) and the charge transfer spectra (R$_{CT}$) of the developed catalysts are given in Figure 4D. As shown in Figure 4C, the smallest R$_s$ and the R$_{CT}$ value for the 1:1 ZnWO4 catalyst signify good electrocatalytic behavior, which is in good agreement with the results obtained through polarization measurements. These results indicate that the zinc tungstate catalyst exhibits low reaction resistance and is a very promising material for water-splitting applications [38].

The electrochemical kinetics of the developed catalyst were studied by exploring the steady-state polarization Tafel curves (Figure 5A). The reaction mechanism and the rate-determining step (RDS) can be accomplished by using the Tafel slope derived from the Tafel equation ($\eta = a + \log j$) with the applied overpotential (η), resulting current density (j mA cm^{-2}), intercept (a), and the Tafel slope (b). The results plotted in Figure 5A demon-

strate the small reaction kinetics for the Pt/C electrode (55.1 mV dec^{-1}) and the 1:1 ZnWO$_4$ electrode (75.3 mV dec^{-1}) compared to those for others, namely the 0.5:1 ZnWO$_4$ electrode (115.0 mV dec^{-1}) and the 2:1 ZnWO$_4$ electrode (145.8 mV dec^{-1}). These findings suggest that the Volmer–Heyrovsky reaction mechanism is involved in the HER process, where proton discharge electron sorption followed by electron desorption occurs. This means that the Volmer step is the RDS, where the HER kinetics follow the charge transfer process from the electrode.
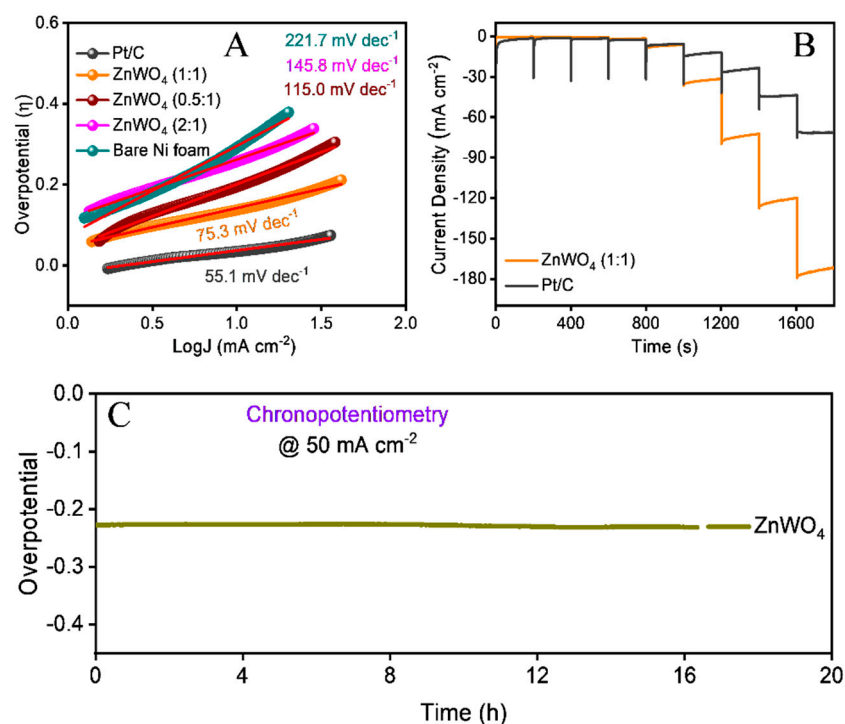
Figure 5. Electrode kinetics for the HER, represented by the Tafel slope (**A**). Consecutive multi-step chronopotentiometry analysis of the 1:1 ZnWO$_4$ catalyst (**B**). Long-term stability analysis of the ZnWO$_4$ catalyst on Ni foam through chronopotentiometry analysis at 50 mA cm^{-2} (**C**).

The practicability and durability of the electrode for HER applications can be tested via stability analysis. Figure 5B shows the consecutive multi-step chronopotentiometric analysis of the 1:1 ZnWO$_4$ and benchmark Pt/C catalysts, where the current responses remain steady throughout the 200 s time period at monotonically increasing applied potentials. The current response of ZnWO$_4$ (1:1) was found to be more consistent than that for the benchmark Pt/C electrode, demonstrating the high practicality of the developed catalyst. This indicates its superior material strength and excellent mass transport during the electrochemical reaction. Moreover, the long-term stability of the ZnWO$_4$ catalyst on Ni foam was evaluated through chronopotentiometric analysis at 50 mA cm^{-2} of applied current, as given in Figure 5C. The result is obvious, showing that there is no significant degradation in the potential response for about 16 h, indicating the robustness of the electrode at a high current density [40]. Overall, the physicochemical and electrochemical results reveal that the tungstate with an equal molar ratio of Zn and W displays exceptional catalytic performance, surpassing the outcomes observed with lower or higher zinc ratios. In this study, we focused on the influence of zinc ions on tungstate regarding its catalytic performance as a green H$_2$ production electrocatalyst. The lower performance of the other electrodes might be associated with reasons such as a lack of saturation of the tungstate at a low content of zinc and the agglomeration of zinc particles at the surface of the tungstate at a higher content of zinc, which will be explored in further research. Based on these

findings, a divalent ion-stabilized tungstate is a good candidate for efficient water-splitting applications for green hydrogen production.

4. Conclusions

In conclusion, strategic divalent ion (Zn^{2+}) modulation on a tungstate ($WO_4{}^{-2}$) moiety results in an ultrathin nanosheet structure with surplus porosity and channels. The electrochemical HER activity is boosted due to the freestanding $ZnWO_4$ nanosheets on Ni foam, and Zn's incorporation effectively modulates the electronic structure and increases the active sites for electroactivity. The optimal integration of Zn ions into the tungstate results in good electrocatalytic performance, which has not yet been investigated. The achievement of a high-performance electrode is made possible through the use of a noble metal-based catalyst (Pt/C). However, this transition metal-based tungstate electrode also demonstrates competitive performance and could be further improved by employing techniques such as defect engineering and heterostructuring. These advancements could enhance its effectiveness in power conversion systems, including water splitting. Hence, our work opens up a low-cost and simple synthesis approach for the design of electrocatalysts in green hydrogen production.

References

1. Luis-Sunga, M.; Regent, L.; Pastor, E.; García, G. Non-Precious Metal Graphene-Based Catalysts for Hydrogen Evolution Reaction. *Electrochem* **2020**, *1*, 75–86. [CrossRef]
2. Pandey, S.; Oh, Y.; Ghimire, M.; Son, J.-W.; Lee, M.; Jun, Y. Value addition of MXenes as photo-/electrocatalysts in water splitting for sustainable hydrogen production. *Chem. Commun.* **2024**, *60*, 8789–8805. [CrossRef] [PubMed]
3. Chen, J.; He, W.; Guo, Y.; Xiao, Y.; Tan, X.; Cui, H.; Wang, C. In situ formed nickel tungsten oxide amorphous layer on metal–organic framework derived $Zn_xNi_{1-x}WO_4$ surface by self-reconstruction for acid hydrogen evolution reaction. *J. Colloid Interface Sci.* **2023**, *652*, 1347–1355. [CrossRef]
4. Zheng, Y.; Jiao, Y.; Jaroniec, M.; Qiao, S.Z. Advancing the Electrochemistry of the Hydrogen-Evolution Reaction through Combining Experiment and Theory. *Angew. Chem. Int. Ed.* **2015**, *54*, 52–65. [CrossRef] [PubMed]
5. Conti, D.M.; Urru, C.; Bruni, G.; Galinetto, P.; Albini, B.; Berbenni, V.; Capsoni, D. High C-Rate Performant Electrospun $LiFePO_4$/Carbon Nanofiber Self-Standing Cathodes for Lithium-Ion Batteries. *Electrochem* **2024**, *5*, 223–242. [CrossRef]
6. Abdin, Z.; Zafaranloo, A.; Rafiee, A.; Mérida, W.; Lipiński, W.; Khalilpour, K.R. Hydrogen as an energy vector. *Renew. Sustain. Energy Rev.* **2020**, *120*, 109620. [CrossRef]
7. Islam, A.; Teo, S.H.; Ng, C.H.; Taufiq-Yap, Y.H.; Choong, S.Y.T.; Awual, M.R. Progress in recent sustainable materials for greenhouse gas (NOx and SOx) emission mitigation. *Prog. Mater. Sci.* **2023**, *132*, 101033. [CrossRef]
8. Perera, F. Pollution from Fossil-Fuel Combustion is the Leading Environmental Threat to Global Pediatric Health and Equity: Solutions Exist. *Int. J. Environ. Res. Public Health* **2017**, *15*, 16. [CrossRef]
9. Chu, S.; Cui, Y.; Liu, N. The path towards sustainable energy. *Nat. Mater.* **2017**, *16*, 16–22. [CrossRef]

10. Ojha, G.P.; Pant, B.; Muthurasu, A.; Chae, S.-H.; Park, S.-J.; Kim, T.; Kim, H.-Y. Three-dimensionally assembled manganese oxide ultrathin nanowires: Prospective electrode material for asymmetric supercapacitors. *Energy* **2019**, *188*, 116066. [CrossRef]

11. Dresselhaus, M.S.; Thomas, I.L. Alternative energy technologies. *Nature* **2001**, *414*, 332–337. [CrossRef]

12. Ding, K.; Li, W.; Li, M.; Bai, Y.; Liang, X.; Wang, H. A Carbon-Particle-Supported Palladium-Based Cobalt Composite Electrocatalyst for Ethanol Oxidation Reaction (EOR). *Electrochem* **2024**, *5*, 506–529. [CrossRef]

13. Kweon, D.H.; Okyay, M.S.; Kim, S.-J.; Jeon, J.-P.; Noh, H.-J.; Park, N.; Mahmood, J.; Baek, J.-B. Ruthenium anchored on carbon nanotube electrocatalyst for hydrogen production with enhanced Faradaic efficiency. *Nat. Commun.* **2020**, *11*, 1278. [CrossRef] [PubMed]

14. Paudel, D.R.; Pan, U.N.; Ghising, R.B.; Kandel, M.R.; Prabhakaran, S.; Kim, D.H.; Kim, N.H.; Lee, J.H. Multi-interfacial dendritic engineering facilitating congruous intrinsic activity of oxide-carbide/MOF nanostructured multimodal electrocatalyst for hydrogen and oxygen electrocatalysis. *Appl. Catal. B Environ.* **2023**, *331*, 122711. [CrossRef]

15. Tian, H.; Cui, X.; Zeng, L.; Su, L.; Song, Y.; Shi, J. Oxygen vacancy-assisted hydrogen evolution reaction of the Pt/WO_3 electrocatalyst. *J. Mater. Chem. A* **2019**, *7*, 6285–6293. [CrossRef]

16. Chang, K.; Tran, D.T.; Wang, J.; Prabhakaran, S.; Kim, D.H.; Kim, N.H.; Lee, J.H. Atomic Heterointerface Engineering of $Ni2P$-$NiSe_2$ Nanosheets Coupled ZnP-Based Arrays for High-Efficiency Solar-Assisted Water Splitting. *Adv. Funct. Mater.* **2022**, *32*, 2113224. [CrossRef]

17. Chen, W.; Pei, J.; He, C.-T.; Wan, J.; Ren, H.; Wang, Y.; Dong, J.; Wu, K.; Cheong, W.-C.; Mao, J.; et al. Single Tungsten Atoms Supported on MOF-Derived N-Doped Carbon for Robust Electrochemical Hydrogen Evolution. *Adv. Mater.* **2018**, *30*, 1800396. [CrossRef]

18. Li, Z.; Ji, S.; Liu, Y.; Cao, X.; Tian, S.; Chen, Y.; Niu, Z.; Li, Y. Well-Defined Materials for Heterogeneous Catalysis: From Nanoparticles to Isolated Single-Atom Sites. *Chem. Rev.* **2020**, *120*, 623–682. [CrossRef] [PubMed]

19. Zhu, J.; Hu, L.; Zhao, P.; Lee, L.Y.S.; Wong, K.-Y. Recent Advances in Electrocatalytic Hydrogen Evolution Using Nanoparticles. *Chem. Rev.* **2020**, *120*, 851–918. [CrossRef] [PubMed]

20. Ganesan, A.; Alhowity, S.; Alsaleh, A.Z.; Guragain, M.; Omolere, O.; Cundari, T.R.; Kelber, J.; D'Souza, F. Electro- and Photocatalytic Conversion of N_2 to NH_3 by Chemically Modified Transition Metal Dichalcogenides, MoS_2, and WS_2. *J. Electrochem. Soc.* **2023**, *170*, 056501. [CrossRef]

21. Zhang, J.; Geng, S.; Li, R.; Zhang, X.; Zhou, Y.; Yu, T.; Wang, Y.; Song, S.; Shao, Z. Novel monoclinic ABO_4 oxide with single-crystal structure as next generation electrocatalyst for oxygen evolution reaction. *Chem. Eng. J.* **2021**, *420*, 130492. [CrossRef]

22. Brijesh, K.; Bindu, K.; Amudha, A.; Nagaraja, H.S. Dual electrochemical application of r-GO wrapped $ZnWO_4$/Sb nanocomposite. *Mater. Res. Express* **2019**, *6*, 115030. [CrossRef]

23. Athar, M.; Fiaz, M.; Farid, M.A.; Tahir, M.; Asghar, M.A.; ul Hassan, S.; Hasan, M. Iron and Manganese Codoped Cobalt Tungstates $Co_{1-(x+y)}Fe_xMn_yWO_4$ as Efficient Photoelectrocatalysts for Oxygen Evolution Reaction. *ACS Omega* **2021**, *6*, 7334–7341. [CrossRef]

24. Brijesh, K.; Bindu, K.; Shanbhag, D.; Nagaraja, H.S. Chemically prepared Polypyrrole/ZnWO4 nanocomposite electrodes for electrocatalytic water splitting. *Int. J. Hydrogen Energy* **2019**, *44*, 757–767. [CrossRef]

25. Pereira, P.F.S.; Gouveia, A.F.; Assis, M.; de Oliveira, R.C.; Pinatti, I.M.; Penha, M.; Gonçalves, R.F.; Gracia, L.; Andrés, J.; Longo, E. $ZnWO_4$ nanocrystals: Synthesis, morphology, photoluminescence and photocatalytic properties. *Phys. Chem. Chem. Phys.* **2018**, *20*, 1923–1937. [CrossRef]

26. Wang, X.; Li, B.; Liu, D.; Xiong, H. $ZnWO_4$ nanocrystals/reduced graphene oxide hybrids: Synthesis and their application for Li ion batteries. *Sci. China Chem.* **2014**, *57*, 122–126. [CrossRef]

27. Sasikumar, R.; Kim, B.; Bhattarai, R.M. Zinc tungstate integrated onto zinc oxide h-MDs-based flexible piezoelectric power device: A new energy technology for real-time indoor laboratory safety warning system. *Chem. Eng. J.* **2024**, *491*, 151889. [CrossRef]

28. Paudel, D.R.; Pan, U.N.; Ghising, R.B.; Dhakal, P.P.; Dinh, V.A.; Wang, H.; Kim, N.H.; Lee, J.H. Interface modulation induced by the 1T Co-WS_2 shell nanosheet layer at the metallic $NiTe2$/Ni core–nanoskeleton: Glib electrode-kinetics for HER, OER, and ORR. *Nano Energy* **2022**, *102*, 107712. [CrossRef]

29. Sultana, F.; Mushtaq, M.; Ferdous, T.; Wang, J.; Lin, M.; Zaman, A.; Althubeiti, K.; Aljohani, M.; Yang, Q. The effect of morphology on electrochemical hydrogen evolution reaction of $ReSe_2$ nano-structures. *New J. Chem.* **2022**, *46*, 14894–14902. [CrossRef]

30. Guragain, M.; Kafle, A.; Adesope, Q.; Altafi, M.K.; Amagbor, S.C.; Mesilov, V.; Kelber, J.A.; Cundari, T.R.; D'Souza, F. Photoenhanced Electrochemical Conversion of Nitrate to Ammonia Via Sulfur Vacancy-Rich Exfoliated MoS_2. *ACS Catal.* **2024**, *14*, 18085–18094. [CrossRef]

31. Anitha, T.; Reddy, A.E.; Durga, I.K.; Rao, S.S.; Nam, H.W.; Kim, H.-J. Facile synthesis of $ZnWO_4$@WS_2 cauliflower-like structures for supercapacitors with enhanced electrochemical performance. *J. Electroanal. Chem.* **2019**, *841*, 86–93. [CrossRef]

32. Kasturi, P.R.; Shanmugapriya, S.; Elizabeth, M.; Athira, K.; Selvan, R.K. Electrocatalytic hydrogen evolution reaction studies of $NiW_{1-x}Mo_xO_4$ (x = 0.0, 0.5 and 1.0) nanoparticles in both acid and alkaline electrolytes. *J. Mater. Sci. Mater. Electron.* **2020**, *31*, 2378–2387. [CrossRef]

33. Luo, F.; Xu, R.; Ma, S.; Zhang, Q.; Hu, H.; Qu, K.; Xiao, S.; Yang, Z.; Cai, W. Engineering oxygen vacancies of cobalt tungstate nanoparticles enable efficient water splitting in alkaline medium. *Appl. Catal. B Environ.* **2019**, *259*, 118090. [CrossRef]

34. Malavekar, D.B.; Lokhande, V.C.; Patil, D.J.; Kale, S.B.; Patil, U.M.; Ji, T.; Lokhande, C.D. Amorphous nickel tungstate films prepared by SILAR method for electrocatalytic oxygen evolution reaction. *J. Colloid Interface Sci.* **2022**, *609*, 734–745. [CrossRef]

35. Muthurasu, A.; Ojha, G.P.; Lee, M.; Kim, H.Y. Zeolitic imidazolate framework derived Co_3S_4 hybridized MoS_2–Ni_3S_2 heterointerface for electrochemical overall water splitting reactions. *Electrochim. Acta* **2020**, *334*, 135537. [CrossRef]

36. Paudel, D.R.; Pan, U.N.; Singh, T.I.; Gudal, C.C.; Kim, N.H.; Lee, J.H. Fe and P Doped 1T-Phase Enriched $WS_2$3D-Dendritic Nanostructures for Efficient Overall Water Splitting. *Appl. Catal. B Environ.* **2021**, *286*, 119897. [CrossRef]

37. De, P.; Halder, J.; Gowda, C.C.; Kansal, S.; Priya, S.; Anshu, S.; Chowdhury, A.; Mandal, D.; Biswas, S.; Dubey, B.K.; et al. Role of porosity and diffusion coefficient in porous electrode used in supercapacitors—Correlating theoretical and experimental studies. *Electrochem. Sci. Adv.* **2023**, *3*, e2100159. [CrossRef]

38. Muthurasu, A.; Ojha, G.P.; Lee, M.; Kim, H.Y. Integration of Cobalt Metal–Organic Frameworks into an Interpenetrated Prussian Blue Analogue to Derive Dual Metal–Organic Framework-Assisted Cobalt Iron Derivatives for Enhancing Electrochemical Total Water Splitting. *J. Phys. Chem. C* **2020**, *124*, 14465–14476. [CrossRef]

39. Wang, Y.Z.; Yang, M.; Ding, Y.-M.; Li, N.-W.; Yu, L. Recent Advances in Complex Hollow Electrocatalysts for Water Splitting. *Adv. Funct. Mater.* **2022**, *32*, 2108681. [CrossRef]

40. Zhai, W.; Ma, Y.; Chen, D.; Ho, J.C.; Dai, Z.; Qu, Y. Recent progress on the long-term stability of hydrogen evolution reaction electrocatalysts. *InfoMat* **2022**, *4*, e12357. [CrossRef]